High-energy, kHz, picosecond hybrid Yb-doped chirped-pulse amplifier

Chun-Lin Chang,[1,4] Peter Krogen,[1,4] Kyung-Han Hong,[1,*] Luis E. Zapata,[2] Jeffrey Moses,[1] Anne-Laure Calendron,[2] Houkun Liang,[1] Chien-Jen Lai,[1] Gregory J. Stein,[1] Phillip D. Keathley,[1] Guillaume Laurent,[1] and Franz X. Kärtner[1,2,3]

[1]*Department of Electrical Engineering and Computer Science and Research Laboratory of Electronics, Massachusetts Institute of Technology (MIT), Cambridge, Massachusetts 02139, USA*

[2]*Centerfor Free-Electron Laser Science, Deutsches Elektronen Synchrotron (DESY), Hamburg, Germany*

[3]*The Hamburg Center for Ultrafast Imaging and Department of Physics, University of Hamburg, Hamburg, Germany*

[4]*These authors contributed equally.*

[*]*kyunghan@mit.edu,*

Abstract: We report on a diode-pumped, hybrid Yb-doped chirped-pulse amplification (CPA) laser system with a compact pulse stretcher and compressor, consisting of Yb-doped fiber preamplifiers, a room-temperature Yb:KYW regenerative amplifier (RGA), and cryogenic Yb:YAG multi-pass amplifiers. The RGA provides a relatively broad amplification bandwidth and thereby a long pulse duration to mitigate B-integral in the CPA chain. The ~1030-nm laser pulses are amplified up to 70 mJ at 1-kHz repetition rate, currently limited by available optics apertures, and then compressed to ~6 ps with high efficiency. The near-diffraction-limited beam focusing quality is demonstrated with M_x^2 = 1.1 and M_y^2 = 1.2. The shot-to-shot energy fluctuation is as low as ~1% (rms), and the long-term energy drift and beam pointing stability for over 8 hours measurement are ~3.5% and <6 μrad (rms), respectively. To the best of our knowledge, this hybrid laser system produces the most energetic picosecond pulses at kHz repetition rates among rod-type laser amplifiers. With an optically synchronized Ti:sapphire seed laser, it provides a versatile platform optimized for pumping optical parametric chirped-pulse amplification systems as well as driving inverse Compton scattered X-rays.

OCIS codes: (140.3615) Lasers, ytterbium; (140.3280) Laser amplifiers; (320.7090) Ultrafast lasers.

References and links

1. Y. Deng, A. Schwarz, H. Fattahi, M. Ueffing, X. Gu, M. Ossiander, T. Metzger, V. Pervak, H. Ishizuki, T. Taira, T. Kobayashi, G. Marcus, F. Krausz, R. Kienberger, and N. Karpowicz, "Carrier-envelope-phase-stable, 1.2 mJ, 1.5 cycle laser pulses at 2.1 μm," Opt. Lett. **37**(23), 4973–4975 (2012).
2. K.-H. Hong, S.-W. Huang, J. Moses, X. Fu, C. J. Lai, G. Cirmi, A. Sell, E. Granados, P. Keathley, and F. X. Kärtner, "High-energy, phase-stable, ultrabroadband kHz OPCPA at 2.1 μm pumped by a picosecond cryogenic Yb:YAG laser," Opt. Express **19**(16), 15538–15548 (2011).
3. S.-W. Huang, G. Cirmi, J. Moses, K.-H. Hong, S. Bhardwaj, J. R. Birge, L. J. Chen, E. Li, B. J. Eggleton, G. Cerullo, and F. X. Kartner, "High-energy pulse synthesis with sub-cycle waveform control for strong-field physics," Nat. Photonics **5**(8), 475–479 (2011).
4. H. Fattahi, H. G. Barros, M. Gorjan, T. Nubbemeyer, B. Alsaif, C. Y. Teisset, M. Schultze, S. Prinz, M. Haefner, M. Ueffing, A. Alismail, L. Vámos, A. Schwarz, O. Pronin, J. Brons, X. T. Geng, G. Arisholm, M. Ciappina, V. S. Yakovlev, D. E. Kim, A. M. Azzeer, N. Karpowicz, D. Sutter, Z. Major, T. Metzger, and F. Krausz, "Third-generation femtosecond technology," Optica **1**(1), 45–63 (2014).
5. C. Manzoni, O. D. Mücke, G. Cirmi, S. Fang, J. Moses, S.-W. Huang, K.-H. Hong, G. Cerullo and F. X. Kärtner, "Coherent pulse synthesis: towards sub-cycle optical waveforms," Laser Photon. Rev. **9**(2), published online (2015).
6. W. S. Graves, J. Bessuille, P. Brown, S. Carbajo, V. Dolgashev, K.-H. Hong, E. Ihloff, B. Khaykovich, H. Lin, K. Murari, E. A. Nanni, G. Resta, S. Tantawi, L. E. Zapata, F. X. Kärtner, and D. E. Moncton, "Compact x-ray

#236053 - $15.00 USD Received 11 Mar 2015; accepted 3 Apr 2015; published 10 Apr 2015

source based on burst-mode inverse Compton scattering at 100 kHz," Phys. Rev. Accel. Beams **17**(12), 120701 (2014).
7. C.-L. Chang, P. Krogen, H. Liang, G. J. Stein, J. Moses, C.-J. Lai, J. P. Siqueira, L. E. Zapata, F. X. Kärtner, and K.-H. Hong, "Multi-mJ, kHz, ps deep-ultraviolet source," Opt. Lett. **40**(4), 665–668 (2015).
8. S.-W. Huang, E. Granados, W. R. Huang, K.-H. Hong, L. E. Zapata, and F. X. Kärtner, "High conversion efficiency, high energy terahertz pulses by optical rectification in cryogenically cooled lithium niobate," Opt. Lett. **38**(5), 796–798 (2013).
9. D. Rand, D. Miller, D. J. Ripin, and T. Y. Fan, "Cryogenic Yb^{3+}-doped materials for pulsed solid-state laser applications," Opt. Mater. Express **1**(3), 434–450 (2011).
10. S. J. Yoon and J. I. Mackenzie, "Cryogenically cooled 946nm Nd:YAG laser," Opt. Express **22**(7), 8069–8075 (2014).
11. D. C. Brown, "The promise of cryogenic solid-state lasers," IEEE J. Sel. Top. Quantum Electron. **11**(3), 587–599 (2005).
12. T. Metzger, A. Schwarz, C. Y. Teisset, D. Sutter, A. Killi, R. Kienberger, and F. Krausz, "High-repetition-rate picosecond pump laser based on a Yb:YAG disk amplifier for optical parametric amplification," Opt. Lett. **34**(14), 2123–2125 (2009).
13. M. Schulz, R. Riedel, A. Willner, T. Mans, C. Schnitzler, P. Russbueldt, J. Dolkemeyer, E. Seise, T. Gottschall, S. Hädrich, S. Duesterer, H. Schlarb, J. Feldhaus, J. Limpert, B. Faatz, A. Tünnermann, J. Rossbach, M. Drescher, and F. Tavella, "Yb:YAG Innoslab amplifier: efficient high repetition rate subpicosecond pumping system for optical parametric chirped pulse amplification," Opt. Lett. **36**(13), 2456–2458 (2011).
14. T. Y. Fan, D. J. Ripin, R. L. Aggarwal, J. R. Ochoa, B. Chann, M. Tilleman, and J. Spitzberg, "Cryogenic Yb^{3+}-doped solid-state lasers," IEEE J. Sel. Top. Quantum Electron. **13**(3), 448–459 (2007).
15. K.-H. Hong, A. Siddiqui, J. Moses, J. Gopinath, J. Hybl, F. O. Ilday, T. Y. Fan, and F. X. Kärtner, "Generation of 287 W, 5.5 ps pulses at 78 MHz repetition rate from a cryogenically cooled Yb:YAG amplifier seeded by a fiber chirped-pulse amplification system," Opt. Lett. **33**(21), 2473–2475 (2008).
16. L. E. Zapata, H. Lin, H. Cankaya, A.-L. Calendron, W. Huang, K.-H. Hong, and F. X. Kaertner, "Cryogenic composite thin disk high energy pulsed, high average power, diffraction limited multi-pass amplifier," Advanced Solid State Lasers Conference Proceedings, AF3A (2013).
17. A. Calendron, L. E. Zapata, H. Cankaya, H. Lin, and F. X. Kärtner, "Optimized temperature/bandwidth operation of cryogenic Yb:YAG composite thin-disk laser amplifier," in Research in Optical Sciences, OSA Technical Digest (online) (Optical Society of America, 2014), paper JW2A.10.
18. L. E. Zapata, D. J. Ripin, and T. Y. Fan, "Power scaling of cryogenic Yb:$LiYF_4$ lasers," Opt. Lett. **35**(11), 1854–1856 (2010).
19. D. A. Rand, S. E. J. Shaw, J. R. Ochoa, D. J. Ripin, A. Taylor, T. Y. Fan, H. Martin, S. Hawes, J. Zhang, S. Sarkisyan, E. Wilson, and P. Lundquist, "Picosecond pulses from a cryogenically cooled, composite amplifier using Yb:YAG and Yb:GSAG," Opt. Lett. **36**(3), 340–342 (2011).
20. K.-H. Hong, C. J. Lai, J. P. Siqueira, P. Krogen, J. Moses, C. L. Chang, G. J. Stein, L. E. Zapata, and F. X. Kärtner, "Multi-mJ, kHz, 2.1 μm optical parametric chirped-pulse amplifier and high-flux soft x-ray high-harmonic generation," Opt. Lett. **39**(11), 3145–3148 (2014).
21. K.-H. Hong, J. T. Gopinath, D. Rand, A. M. Siddiqui, S. W. Huang, E. Li, B. J. Eggleton, J. D. Hybl, T. Y. Fan, and F. X. Kärtner, "High-energy, kHz-repetition-rate, ps cryogenic Yb:YAG chirped-pulse amplifier," Opt. Lett. **35**(11), 1752–1754 (2010).
22. X. Fu, K.-H. Hong, L.-J. Chen, and F. X. Kärtner, "Performance scaling of high-power picosecond cryogenically cooled rod-type Yb:YAG multipass amplification," J. Opt. Soc. Am. B **30**(11), 2798–2809 (2013).
23. A. H. Curtis, B. A. Reagan, K. A. Wernsing, F. J. Furch, B. M. Luther, and J. J. Rocca, "Demonstration of a compact 100 Hz, 0.1 J, diode-pumped picosecond laser," Opt. Lett. **36**(11), 2164–2166 (2011).
24. K. Ogawa, Y. Akahane, M. Aoyama, K. Tsuji, S. Tokita, J. Kawanaka, H. Nishioka, and K. Yamakawa, "Multi-millijoule, diode-pumped, cryogenically-cooled Yb:$KY(WO_4)_2$ chirped-pulse regenerative amplifier," Opt. Express **15**(14), 8598–8602 (2007).
25. A.-L. Calendron, H. Cankaya, and F. X. Kärtner, "High-energy kHz Yb:KYW dual-crystal regenerative amplifier," Opt. Express **22**(20), 24752–24762 (2014).

1. Introduction

Ultrafast high-power Yb-doped lasers have been proven to be a promising candidate for pumping a variety of nonlinear optical processes, ranging from ultrabroadband optical parametric chirped-pulse amplification (OPCPA) systems [1,2] and multi-color pulse synthesizers [3–5] to compact coherent X-ray sources based on inverse Compton scattering [6]. In particular, ultrafast Yb-based lasers have shown to be particularly well suited to these applications due to their ability to be pumped by readily available high power diode lasers, and their intrinsically high efficiency made possible by their long fluorescence lifetime and low quantum defect. Furthermore, efficient nonlinear frequency conversion techniques to the deep-ultraviolet [7] to the terahertz [8] using ps or sub-ps Yb-doped amplifiers have been

#236053 - $15.00 USD Received 11 Mar 2015; accepted 3 Apr 2015; published 10 Apr 2015

demonstrated. These applications place ever increasing demands on the performance of the laser systems used to drive them, so scaling the pulse energy and average power while maintaining excellent beam profile and stability is a key step towards enabling these new technologies.

Two primary challenges in the design of high power ultrafast lasers are 1) preventing damage in the laser system due to the high peak powers and 2) extracting heat generated in the gain medium. The use of chirped-pulse amplification (CPA) has, for the most part, allowed designers to avoid issues relating to optical damage in these lasers. By chirping the pulse in the amplifier to over 100-1000 times longer than at the output of the laser system, the peak power is significantly reduced to acceptable levels, at the expense of added complexity of the stretching/compression stages. However, to scale to higher average powers, one must also deal with the heat generated in the gain medium due to various inefficiencies in the laser.

Yb-doped materials [9] support emission bandwidths broad enough for the generation of ultrafast pulses while having a distinct advantage in this respect due to their small quantum defect (~9%) compared to Nd:YAG [10] (24%) and Ti:sapphire [11] (34%), as indicated by the ratio of pump wavelength to emission wavelength in Table 1, (λ_p, λ_L respectively). Although the thermal conductivity of Ti:sapphire is much higher than Yb-doped materials, the thermal load per output power is still much lower for Yb-doped materials. This property has allowed Yb-based laser systems to scale to high average powers, and the use of creative designs such as thin-disk [12] or Innoslab [13] geometries have made amplifiers outputting few-ps pulses with multi-tens of mJ at kHz repetition rates possible. Another approach is to take advantage of the fact that when operating at cryogenic temperature, certain key properties of Yb-doped laser media dramatically improve [14]. First, the thermo-optic effect significantly decreases because of the higher thermal conductivity (κ), the lower thermo-optic coefficient (dn/dT), and the lower coefficient of thermal expansion. Second, the gain medium is converted from a three-level system to a quasi-four-level system due to the thermal depopulation of the lower laser level, which decreases the amplification threshold and enhances the efficiency. Third, the cross sections of both the absorption (σ_a) and the emission (σ_e) are significantly increased; furthermore the absorption bandwidth remains sufficiently broad for high power diode pumping at 940 or 980 nm and the emission bandwidth remains sufficiently broad for amplification of ps or sub-ps pulses. Cryogenic cooling allows output powers of hundreds of watts [15], while maintaining good beam quality with relatively simple amplifier configurations, or can even be combined with thin-disk technologies [16] to further push performance [17].

One main limitation of Yb-doped materials, compared to Ti:sapphire, is the relatively narrow gain bandwidth ($\Delta\lambda$), which limits the achievable compressed pulse duration and complicates the pulse stretching required for CPA operation. This can be mitigated through clever selection of the laser host material: for example Yb:YLF [18] is a promising candidate for broadband amplification, with its broad gain bandwidth and long lifetime. It has also been shown that using multiple gain materials, for example Yb:YAG/Yb:GSAG [19], can further improve the performances. Among the common Yb-doped materials shown in Table 1, cryogenically cooled Yb:YAG is particularly well suited for applications requiring both energy and power scaling due to its relatively long fluorescence lifetime, high emission cross section, and its particularly high thermal conductivity, and has been shown to produce tens of mJ pulse energies at kHz repetition rates [20].

The narrowed gain bandwidth of cryogenically cooled Yb:doped materials further complicates the pulse stretching/compression, and has been a main limiting factor in our previous kHz-repetition-rate systems [20,21], which are based on a cryogenic Yb:YAG regenerative amplifier (RGA) and cryogenic Yb:YAG multipass amplifiers (MPA). Due to the narrow bandwidth (<0.24 nm FWHM) output from a cryogenic Yb:YAG RGA [21], it is challenging to chirp the pulses enough to avoid surface damage and B-integral related issues. We can mitigate this issue by increasing the stretching ratio and/or increasing the spectral

#236053 - $15.00 USD Received 11 Mar 2015; accepted 3 Apr 2015; published 10 Apr 2015

bandwidth [22]. A large stretching ratio of approximately ~0.8 ns/nm has been already achieved using a compact stretcher based on multiple chirped volume Bragg gratings (CVBGs) [21], but due to the high peak powers of the amplified pulses it is not possible to use CVBGs for the recompression, so we use a traditional grating compressor. Since the large stretching ratio already necessitates a bulky compressor (with a grating separation of ~5 meters in our case), it is undesirable to further chirp the pulses by increasing the stretching ratio. Instead, we employ a room-temperature Yb:KYW RGA to take advantage of a significantly broader emission bandwidth of the Yb:KYW crystal (~18 nm) over that of the cryogenic Yb:YAG crystal (<1.5 nm). While a similar configuration using a room-temperature Yb:YAG RGA has already shown great promise for low-repetition-rate CPA systems (10–100 Hz) allowing the generation of greater than 100 mJ few-ps duration pulses [23], we show that it can be of great advantage for kHz systems as well.

Table 1. Characteristics of different laser crystals

Laser crystal	τ_L (ms)	$\sigma_a \setminus \sigma_e$ (pm^2)	$\lambda_p \setminus \lambda_L$ (nm)	$\Delta\lambda$ (nm)	κ ($W \cdot K^{-1} m^{-1}$)	dn/dT (μK^{-1})	T (K)
Ti:sapphire	0.0032 0.0039	4.5 \ 41 -	495\790	~200 -	33 1000	12.8 1.9	300 77
Nd(1%):YAG	0.23 -	6.9 \ 28 16.9 \ -	808\1064	~0.6 -	14 51	7.8 0.9	300 77
Yb(2%):YAG	0.95 0.85	0.9 \ 2.4 2.77 \ 11.00	941\1030	~11 <1.5	10.6(5.7) 39	8.62 0.9	300 80
Yb(5%):YLF (‖c)	2.08 1.99	1.06 \ 0.75 6.97 \ 1.80	959\1017	>30 ~8	5.2 13.7	–1.8 –6.6	300 77
Yb(5%):KYW (‖a)	0.32 -	18.3 \3.00 - \ 6.00	981\1028	~18 ~6	3.3 7.4	0.4 -	300 77
Yb(2%):GSAG	-	-\5.00	969\1030	- ~2.4	4.76 11.6	5.2 -	300 77

Ref [9–11], [14], [18,19], [24,25].

In this paper, we develop and fully characterize a high-energy, kHz, picosecond, hybrid Yb-doped CPA laser system with all optical synchronization to a Ti:sapphire seed oscillator for pumping an OPCPA laser systems or other nonlinear optical experiments. Using a room-temperature bulk Yb:KYW RGA rather than a cryogenic Yb:YAG RGA, we provide a broader bandwidth, longer chirped-pulse seeder for the two subsequent cryogenic rod-type Yb:YAG MPA to maintain a spectral bandwidth as broad as 0.35 nm throughout the amplifier. In addition, the maximum uncompressed energy reaches 70 mJ, currently limited by the available optical apertures and not by B-integral, at 1 kHz repetition rate with excellent shot-to-shot and long term stabilities in energy. We show compression to a pulse duration of 5.9 ps with an 80% throughput, corresponding to 1.2 times the transform-limited duration with a peak power exceeding 8 GW. The corresponding beam propagation factors are M_x^2 = 1.1 and M_y^2 = 1.2, close to the diffraction limit. The laser demonstrated here provides a versatile platform optimized for pumping OPCPA systems as well as driving inverse Compton scattered X-rays.

2. System layout of the picosecond hybrid Yb-doped CPA laser

The hybrid Yb-doped CPA laser system is composed of a seed oscillator, three Yb-doped pre-amplifiers, a stretcher, a room-temperature Yb:KYW RGA, two cryogenic Yb:YAG MPA, and a pulse compressor. The main laser architecture follows our previous works [2,20] and is optimized for pumping ultrabroadband OPCPA systems. Figure 1 shows the experimental layout of the entire CPA laser system. An octave-spanning Ti:sapphire oscillator (Octavius-85M, IdestaQE/Thorlabs) generates few-cycle femtosecond laser pulses with an average power of ~200 mW at 85-MHz repetition rates, which are used to seed the OPCPA system [3]. Approximately 90% of the light in the spectral range from 1010 nm to 1060 nm, corresponding to ~2 mW of average power, is extracted and amplified in a single-mode (SM)

#236053 - $15.00 USD Received 11 Mar 2015; accepted 3 Apr 2015; published 10 Apr 2015

Yb-doped fiber amplifier (YDFA), as indicated as YDFA 0 in Fig. 1. We then narrow the spectral range to a ~4 nm bandwidth centered at ~1030 nm using a bandpass filter, and amplify in YDFA 1 indicated in Fig. 1 to precompensate for the losses in the stretcher. The compact stretcher consists of a pair of CVBGs with a chirp rate of ~100 ps/nm per bounce over a 2-nm operation bandwidth (for each CVBG). The total footprint is 20 cm by 15 cm. After 8 bounces off the CVBGs (Ondax Inc.), giving a total chirp rate of ~800 ps/nm, we obtain positively-chirped pulses with a temporal width of ~680 ps at FWHM, determined by the measured spectrum of the stretched pulses as shown in Fig. 2(b). The reflection loss in the CVBG stretcher is compensated by YDFA 2 in Fig. 1, and a pulse energy of ~0.5 nJ at 85 MHz is delivered to the input of RGA. A fiber polarization controller is used to ensure the linear polarization of the pulses from the non-polarization-maintaining YDFA and a Faraday isolator is used to protect the YDFA chain from the RGA.

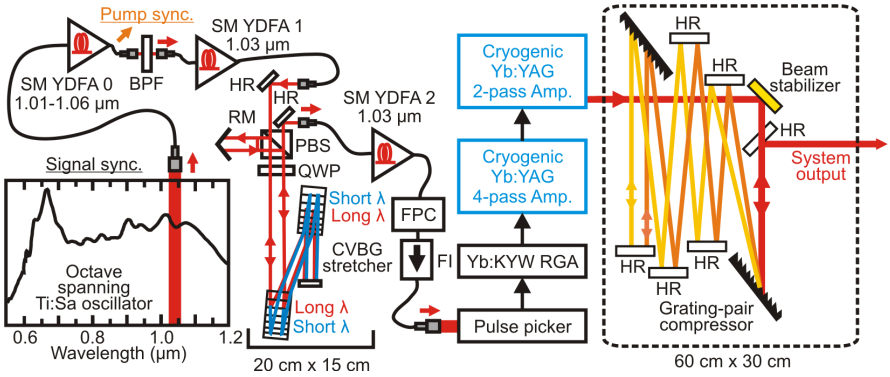

Fig. 1. Experimental layout of picosecond hybrid Yb-doped chirped-pulse amplifier laser system. SM YDFA, single-mode Yb-doped fiber amplifier; BPF, bandpass filter; HR, high-reflection mirror; RM, roof mirror, PBS, polarization beam splitter; QWP, quarter-wave plate; CVBG, chirped volume Bragg grating; FPC, fiber polarization control; FI, Faraday isolator; RGA, regenerative amplifier.

After amplification in the subsequent Yb:KYW and Yb:YAG amplifiers, which will be described in the next sections, the laser pulses are compressed using a pair of dielectric-coated diffraction gratings with a dimension of 9.0 cm by 3.5 cm in width by height. The grating groove density and diffraction efficiency of the gratings is 1752 lines/mm and 95%, respectively. The multi-layer dielectric coating (performed at Lawrence Livermore National Laboratory) provides a damage threshold of >2 J/cm^2 for ps pulses and a thermal deformation threshold of ~1 kW/cm^2 (CW) within an operation bandwidth of ~10 nm. We set an angle of incidence of 59° into the first grating and use multiple bounces off additional dielectric mirrors to achieve the required separation of ~4.92 m between gratings in a footprint area of 60 cm by 30 cm. The measured compression throughput is ~80%. Furthermore, the first turning mirror before the pulse compressor is equipped with piezo-electric actuators, and is used with an active beam stabilization system (Thorlabs Inc.) to lock the position of the beam at the experiment to reduce the short-term fluctuations of beam pointing and eliminate the long-term pointing drift.

3. Room-temperature Yb:KYW RGA for larger bandwidth

As a gain medium Yb:KYW is a good candidate for producing the seed signal for Yb:YAG amplifiers because its gain bandwidth is broad, spanning the range from 1024 to 1042 nm, and is well overlapped with that of Yb:YAG. Table 1 indicates that both its cross sections and thermal conductivity are also high and, while its lifetime is shorter than Yb:YAG, it is still acceptable for kHz operation with a CW pump. Furthermore, Yb:KYW at both cryogenic

#236053 - $15.00 USD Received 11 Mar 2015; accepted 3 Apr 2015; published 10 Apr 2015

temperatures [24], and more recently at room temperature [25] has already been used to produce the multi-mJ level output needed for seeding booster amplifiers.

The first stage of the main amplifier chain is a commercial, ~2 mJ, bulk Yb:KYW RGA (s-pulse HP^2, Amplitude Systémes). A pulse picker based on a Pockels cell is used to reduce the repetition rate from 85 MHz to 1 kHz to suppress the amplification of multiple pulses in the RGA. The intracavity pulse buildup and output energy are monitored using a fast photodiode from the resonator leakage through the end mirror of the RGA. At a total pump power of ~39 W from two 980-nm diode lasers, the RGA output energy vs. the input seed energy is shown in Fig. 2(a). The output pulse starts saturating at ~1.0 mJ as the input pulse energy is increased to >0.1 nJ. At an input energy of 0.5 nJ, an output energy of 1.7 mJ is obtained with a shot-to-shot fluctuation of ~0.2%. The resulting gain and extracted efficiency are 65.2 dB and 4.3%, respectively. The near-field profile of the output beam shows a $1/e^2$ diameter of 2.1 mm and 3.0 mm along the horizontal (x) and vertical (y) direction, respectively.

Figures 2(b) and 2(c) show the normalized spectra centered at ~1030.5 nm from the input and output of RGA, respectively. The spectrum reflected from the CVBG stretcher shown in Fig. 2(b) has a large amplitude modulation caused by the slight spatial chirp due to fabrication errors in the CVBGs. Because of a broad emission bandwidth of ~18 nm for the Yb:KYW gain medium at room temperature, the gain narrowing in the high-gain RGA is very mild, and thus the output bandwidth is approximately the same as the ~1 nm bandwidth from the stretcher. The output is slightly shifted to shorter wavelengths because the peak of the Yb:KYW gain is located at ~1028 nm whereas this system operates a 1030.5 nm. The chirped duration of the pulses, however, remains ~740 ps. In the previous cryogenic Yb:YAG RGA operation, the output spectral bandwidth was as narrow as 0.24 nm [2] because of the limited emission bandwidth of <1.5 nm for the Yb:YAG gain medium at cryogenic temperatures.

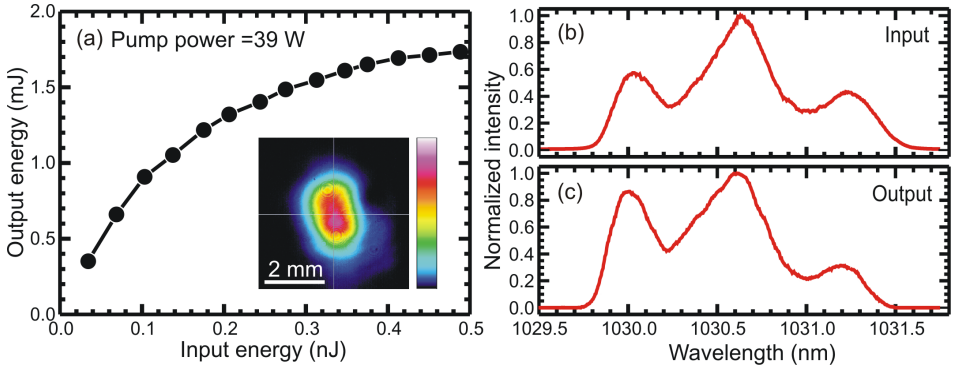

Fig. 2. The output energy of Yb:KYW RGA vs. input seed energy at the diode pump power of 39 W (a), and the normalized spectral distribution from the input (b) and output (c). The inset is the near-field image of beam profile at RGA output.

4. Cryogenic Yb:YAG multi-pass amplifiers for power scaling

Two cryogenically-cooled rod-type Yb:YAG MPAs boost the pulse energy up to 70 mJ at a 1-kHz repetition rate. The first stage uses a collinear four pass configuration using a Faraday rotator to obtain a relatively high gain of ~15. Due to the lack of a Faraday rotator with large enough aperture, the second stage has a collinear double-pass configuration to achieve a moderate gain of ~3.5.

4.1 Four-pass amplifier for high-gain operation

Figure 3 shows the experimental setup of the first-stage four-pass cryogenic Yb:YAG amplifier. A Galilean telescope is used as a beam expander with a magnification of 1.5 for mode-matching the output of the RGA into the amplifier. The collinear four-pass geometry

#236053 - $15.00 USD Received 11 Mar 2015; accepted 3 Apr 2015; published 10 Apr 2015

was realized by polarization multiplexing: the first two passes are achieved using a thin-film polarizer (TFP) and a quarter-wave plate (QWP), while the next two passes are completed using an additional TFP, a half-wave plate (HWP) and a Faraday rotator. To counteract the thermal lensing in the gain medium, an additional pair of lenses ($f = -20$ cm and $f = +25$ cm, with a spacing of 2.7 cm), which act as a variable focal length lens, were inserted before the end mirror (optically between the second and third passes in the amplifier).

For the first cryogenic amplifier, a 1-at.% doped Yb:YAG crystal (10-mm long, with 2-mm-long undoped endcaps on both sides) is mounted in a Dewar with a pressure maintained below ~10^{-6} Torr. The crystal is indium-bonded to a sapphire heat sink that is attached to a copper base plate which contacts with the liquid nitrogen for cooling by boiling. The heat sink helps to minimize thermal stress during the thermal cycling from cryogenic temperatures to room temperature. The liquid nitrogen is automatically refilled for continuous operation. A 2*f*-2*f* image system is installed for monitoring the spatial overlap between the pump beam and the amplified beam at the crystal. The image of the pump beam at the crystal in the inset of Fig. 3 shows a near flat-top profile with a $1/e^2$ diameter of 3.0 mm. The signal beam size of 6.2 mm in $1/e^2$ diameter decreases to 2.2 mm after amplification, due to gain guiding and residual thermal lensing. The 940-nm pump beam from a laser diode is delivered through a multimode fiber with a diameter of 600 μm and is imaged to the Yb:YAG crystal using a collimator of $f = 5$ cm and a focusing lens of $f = 25$ cm. The pump absorption is relatively low at ~75% due to the central wavelength of the diode pumps being slightly higher than the absorption peak at 940nm. A Galilean telescope with a magnification of 1.5 expands the amplified beam for the next amplifier stage.

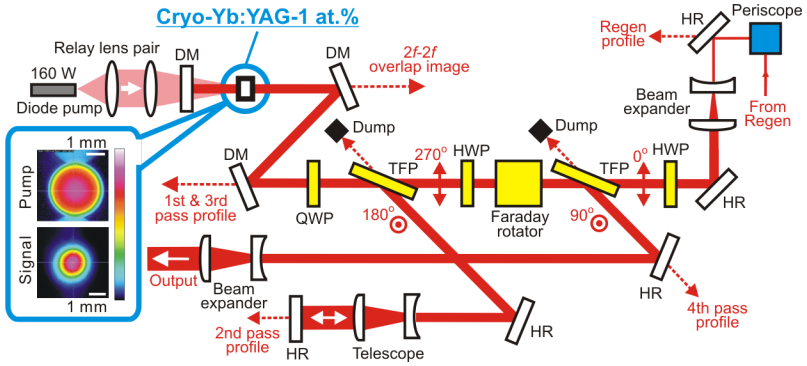

Fig. 3. Optical layout of diode-pumped picosecond cryogenic Yb:YAG 4-pass amplifier. DM, dichroic mirror; QWP, quarter wave plate; HWP, half wave plate; TFP, thin film polarizer; HR, high-reflection mirror. The inset shows the images of the beam profiles at the crystal of pump (upper) and amplified signal (lower).

We characterized the amplification performance of the four-pass amplifier in various conditions. Figure 4 shows the gain, extraction efficiency, and energy stability for different pump powers or seed energies. In Fig. 4(a), at a fixed pump power of ~170 W the amplifier gain drops from 62.5 to 14.2 while the extraction efficiency increases from 0.4% to 12% as the input energy is increased to the maximum of ~1.5 mJ. Furthermore, the saturation naturally improves the energy stability, which can be seen in Fig. 4(b). The measured shot-to-shot energy fluctuation (ΔE/E) drops from 2.5% to 1.1% (rms, measured over a 10 s period) with increasing seed energy.

Figure 4(c) shows the output pulse energy reaches to 22.1 mJ corresponding to an extraction efficiency of ~13% as the pump power is increased to 170 W at a fixed input energy of 1.5 mJ. The extraction efficiency starts to saturate at a pump power of >150 W with a saturated slope efficiency of ~0.3. The inset of Fig. 4(c) shows the near-Gaussian output beam profile with a $1/e^2$ diameter of ~2.7 mm, measured under full operation from the mirror

#236053 - $15.00 USD Received 11 Mar 2015; accepted 3 Apr 2015; published 10 Apr 2015

leakage after four passes as shown in Fig. 3. The maximum output energy can reach to >30 mJ if the pump power is increased to 250 W, but for long term operation we operate the amplifier at 22 mJ of output energy.

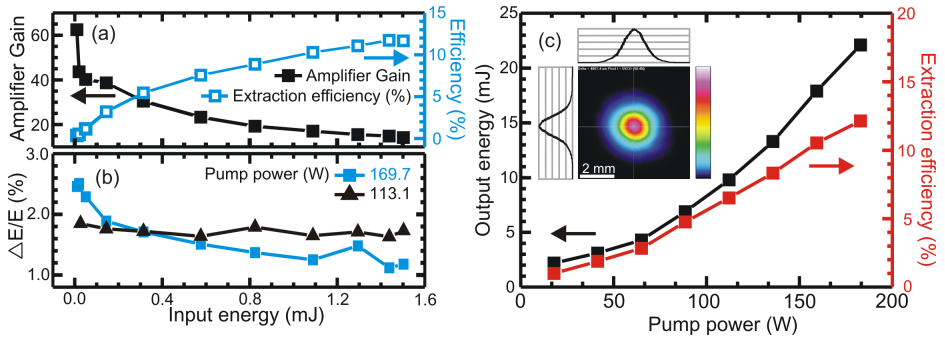

Fig. 4. For cryogenic Yb:YAG 4-pass amplifier, (a) the amplitude gain and extracted efficiency and (b) the corresponding energy fluctuation (ΔE/E) vs. input energies; (c) The output energy and extracted efficiency vs. pump powers. The inset shows the near-field image of output beam and the corresponding 2D lineout after four passes.

4.2 Two-pass amplifier for high efficiency energy extraction

The second cryogenic Yb:YAG amplifier is set up in a two-pass configuration, as shown in Fig. 5. The periscope rotates the beam image by 90° for compensating the thermally induced astigmatism from the 4-pass amplifier, and then a HWP recovers the horizontal polarization. The two-pass geometry is achieved by polarization multiplexing using the same technique as in the first amplifier. A single negative lens (f = −100 cm) is placed before the Yb:YAG crystal to compensate for the thermal lensing in this amplifier. Before entering the pulse compressor, the amplified beam is expanded using a Galilean telescope with a magnification of 1.25.

We use a 2-at.% doped Yb:YAG crystal (15-mm long, with a 2-mm-long undoped endcap on pumping side), which is also mounted in a vacuum Dewar and cryogenically cooled by liquid nitrogen. The pump beam is also delivered by a 600 μm-diameter multi-mode fiber and the image at the fiber facet is relayed to the crystal with a magnification of ~6, and the pump absorption is >95% at ~940 nm. The inset of Fig. 5 shows the image of the near-flat-top pump beam profile with a $1/e^2$ diameter of ~3.9 mm (top). In the crystal, the $1/e^2$ diameter of the signal beam profile decreases from 3.7 mm to 3.1 mm after amplification.

The performance of the amplifier in terms of gain and energy extraction versus input energy and pump power is characterized. Figure 6(a) shows that the amplifier gain at a specific pump power of ~160 W decreases from 7.9 to 3.0 while the corresponding extracted efficiency jumps from 1.1% to 24.5% in two passes when the input energy is increased to the maximum of ~19.6 mJ with only minor loss from the 4-pass amplifier. The alignment was finely optimized for the thermal condition at ~160 W. Figure 6(b) shows the corresponding energy fluctuation ΔE/E which drops from 2.1% to 1.0% with increasing amplifier saturation. Figure 6(c) shows the output energy versus pump power when the input energy is fixed at ~20 mJ. The maximum pulse energy of 70 mJ was obtained at a pump power of ~186 W with a corresponding extraction efficiency of 27%. In the inset of Fig. 6(c), the output beam profile with a $1/e^2$ diameter of ~4.5 mm is measured under full operation through the mirror leakage after two passes as shown in Fig. 5.

#236053 - $15.00 USD Received 11 Mar 2015; accepted 3 Apr 2015; published 10 Apr 2015

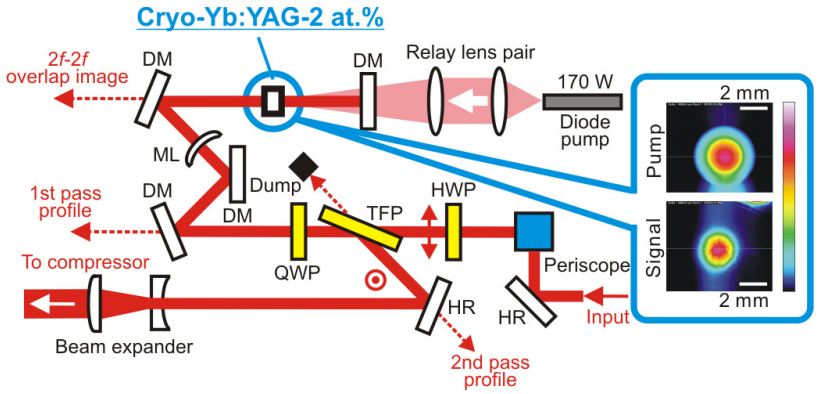

Fig. 5. Optical layout of the diode-pumped picosecond cryogenic Yb:YAG 2-pass amplifier. ML, Meniscus lens. The inset at right side is the far-field images of the beam profiles at the crystal of pump (upper) and amplified signal (lower).

It should be noted that damage of the Dewar window on the pumping side occasionally occurs during operation at 70 mJ. Therefore, we maintain the output energy at <60 mJ for daily operations. Increasing the beam size at the crystal along with larger-aperture optics or a longer stretching can help to boost the output energy beyond 100 mJ from the current configuration of the amplifier chain. Finally, since the lifetime of Yb:YAG is comparable to the repetition period (0.85 ms vs 1 ms), increasing the repetition rate to multi-kHz should further increase the extraction efficiency.

5. Output characteristics of the hybrid CPA laser system

In this section, the systematic measurements of the output characteristics of amplified pulses are presented, including the long-term stability of energy and beam pointing, the evolution of beam propagation factor and spectral distribution, and the spatial beam profile and temporal distribution after compression.

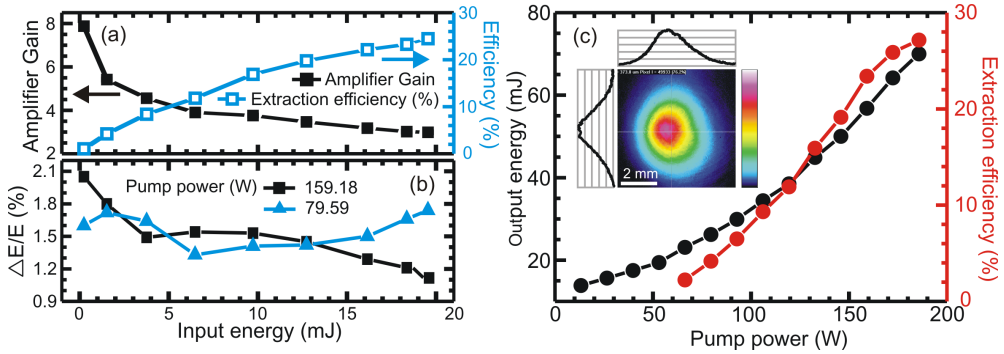

Fig. 6. For cryogenic Yb:YAG 2-pass amplifier, (a) the amplitude gain and extracted efficiency, and (b) the corresponding energy fluctuation (ΔE/E) vs. input energies; (c) The output energy and extracted efficiency vs. pump powers with ~20 mJ input energy. The inset shown in Fig. 6(c) is the near-field image from the output of the two-pass amplifier.

5.1 Long-term stability of energy and beam pointing

Long-term stability of the amplifier chain is crucial as a pump laser for OPCPA systems and eventually for its applications to demanding pump-probe experiments. Figure 7(a) shows the long-term energy stability recorded every one second from the output of the amplifier chain before compression over >8 hours using a pyroelectric energy sensor (NOVA II, Ophir Inc.) without any averaging. We found that the short term energy stability was approximately 1%

#236053 - $15.00 USD Received 11 Mar 2015; accepted 3 Apr 2015; published 10 Apr 2015

rms (10-s period, 10,000 measurements), and that the long term stability over an 8-hour period was 3.5% rms. The inset of Fig. 7(a) shows the histogram of the shot-to-shot fluctuations in the first 60 records in one minute. The long-term drift is mostly caused by temperature oscillations in the laboratory.

After the pulse compressor, the long-term beam pointing stability, shown in Fig. 7(b), was recorded by a charge-coupled device (CCD; WinCamD, Dataray Inc.) placed approximately 10 meters after the second cryogenic Yb:YAG gain medium, where an OPCPA crystal is located. The beam diameter at this point is 2.2 mm, and the pointing stability is measured to be 1.8 μrad rms in the horizontal direction and 6 μrad rms in the vertical direction, which is dominated by high-frequency fluctuations and has negligible long term drift. This represents a fluctuation of <2.7% of the full angle divergence of the beam.

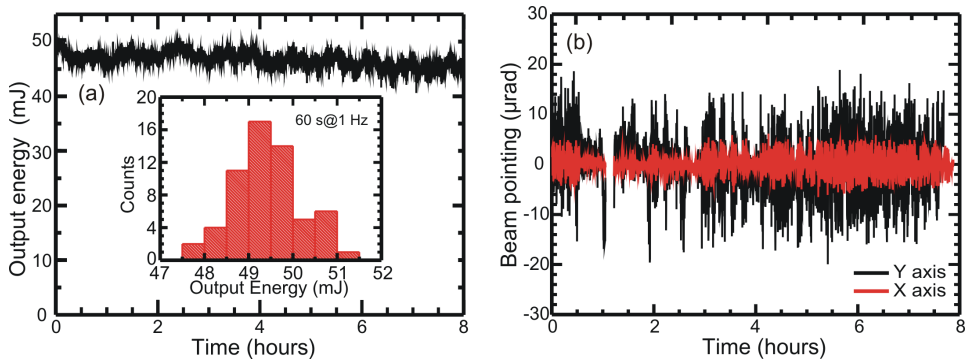

Fig. 7. For long-term measurements for more than 8 hours, (a) the output energy and (b) The beam pointing vs. time in both horizontal (x) and vertical (y) axes with active beam stabilizer. The inset in (a) is the histogram of shot-to-shot fluctuation in the first 60 measurements in 1 minute.

5.2 Evolution of focused beam quality (M^2 values)

The degradation of the amplified beam quality due to thermo-optic effects and nonlinear effects can be evaluated by measuring the beam propagation factor, M^2 value, at each amplifier stage. Figure 8 shows the evolution of M^2 values measured after each amplifier chain. For the M^2 measurements we picked up the collimated laser beam from the mirror leakage and then loosely focused the beam using an f = 100 cm plano-convex lens to get a large and resolvable spot size. A CCD recorded the entire evolution of the transverse beam profile along the beam propagation direction. The fitting curves based on Gaussian beam propagation give M^2 values for each of the amplifier stages. Since the Yb:KYW RGA is seeded by SM YDFAs, the initial M^2 can be ideally considered as 1.

Figure 8(a) shows that the results measured from the commercial Yb:KYW RGA are M_x^2 = 1.22 and M_y^2 = 1.17 and the far-field profile of a focal spot shown in the inset image is slightly elliptical. However, the cryogenic Yb:YAG four-pass amplifier filters out the beam profile with a guided gain profile in the crystal and therefore produces a more symmetric profile than the input beam, as shown in the inset of Fig. 8(b), with excellent M^2 values of M_x^2 = 1.06 and M_y^2 = 1.06. The good beam quality is maintained in the double-pass amplifier and the compressor. We obtained M_x^2 = 1.13 and M_y^2 = 1.21 for compressed pulses, as shown in Fig. 8(c). The far-field profile in the inset image of Fig. 8(c) is still symmetric and the growth of the M^2 value through the double-pass amplifier and the compressor is only 1.1 times. The M^2 grows slightly faster in y direction, owing to the unidirectional heat dissipation at the crystal.

#236053 - $15.00 USD Received 11 Mar 2015; accepted 3 Apr 2015; published 10 Apr 2015

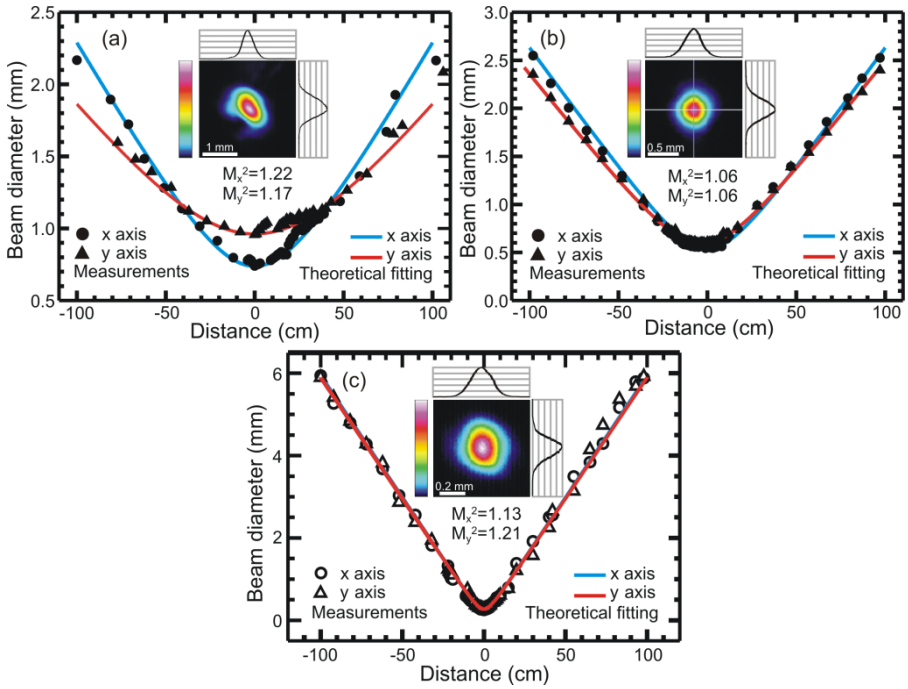

Fig. 8. The evolution of beam propagation factor from (a) the Yb:KYW RGA, (b) the cryogenic Yb:YAG four-pass amplifier, to (c) the compressor output after the cryogenic Yb:YAG two-pass amplifier. The insets are the far-field images of focal spot profile focused by an f = 100 cm lens with a lineout of beam profile in two dimensions.

5.3 Evolution of spectral profile

We also characterized the spectral profile at each amplifier stage. Figure 9(a) presents the amplified spectra after two passes and then four passes in the four-pass amplifier. Compared to the output spectrum of the Yb:KYW RGA shown in Fig. 2(c), the gain spectrum of cryogenic Yb:YAG is centered at 1030.5 nm with a bandwidth ~1.5 nm. The pedestal at 1031.3 nm decreases to a level close to background after two passes because it is out of the amplification bandwidth. In the next two passes, the spectral profile continues to become slightly narrower, due to the effect of gain narrowing, while the pedestal at 1030.0 nm is suppressed. The same tendency appears in the following double-pass amplifier, as shown in Fig. 9(b). The pedestal at 1030.0 nm gets weaker, as the gain narrowing continues.

Figure 9(c) summarizes the evolution of the spectral bandwidth of positively-chirped pulses measured at each stage after the CVBG stretcher. The central wavelength through the entire amplifier chain is fixed at ~1030.5 nm. As previously mentioned, the Yb:KYW RGA reshapes the spectrum and the FWHM spectral bandwidth increases from 0.85 nm to 0.93 nm. In the first two passes of the four-pass amplifier, the spectral bandwidth decreases to 0.54 nm due to the gain narrowing of the cryogenic Yb:YAG and further decreases to 0.45 nm in the next two passes. Finally, the spectral bandwidth after the double-pass amplifier becomes 0.35 nm, corresponding to a stretched duration of ~280 ps. Compared to the all-cryogenic Yb-doped amplifier chain [20], we obtain 1.8 times broader spectral bandwidth and pulse duration of chirped pulses from the current hybrid Yb-doped CPA chain. The longer pulse duration helps the power and energy scaling of this CPA chain by mitigating both the nonlinear phase (B-integral) and surface damage issues. The operation bandwidth of the pulse stretcher can be further optimized to generate broader spectral bandwidth of amplified pulses from the hybrid amplifier chain. It is noted that the center wavelength is offset by ~1.5 nm from that in our

#236053 - $15.00 USD Received 11 Mar 2015; accepted 3 Apr 2015; published 10 Apr 2015

previous reports (~1029.0 nm) [2,15,20] due to the calibration difference between optical spectrum analyzers.

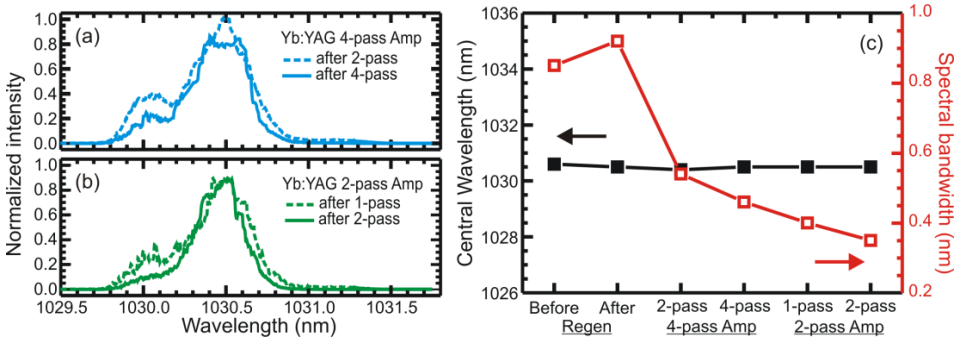

Fig. 9. The output optical spectra of (a) Yb:YAG 4-pass amplifier and (b) Yb:YAG 2-pass amplifier; (c) The evolution of central wavelength and spectral bandwidth during amplification.

5.4 Temporal profile after compression

The temporal profile of the compressed picosecond laser pulses is characterized using an autocorrelator (*pulse*Check 50, APE GmbH). In the grating-pair pulse compressor, the angle of incidence on the first grating is fixed at 59 degrees and the grating separation is scanned while the diffraction angle to the second grating is finely adjusted. By optimizing the angle to ~70 degrees for the second grating at a grating separation of 4.92 m, we obtained the shortest FWHM width of autocorrelation trace of 8.4 ps with a negligible pedestal, as shown in Fig. 10(b). The corresponding FWHM pulse duration is 5.9 ps with a Gaussian fit, which is ~1.2 times the transform limit. When the angle is intentionally detuned by around −1 and + 1 degree, the FWHM width of the autocorrelation trace becomes 15.6 ps (11.0 ps of pulse duration) and 18.2 ps (12.8 ps of pulse duration), shown in Figs. 10(a) and 10(c), respectively, where the resulting temporal pulse duration becomes longer with positive and negative chirp. Due to the narrow spectral bandwidth the spatial chirp is negligible in these cases. The clean compressed pulse shape without the pedestal indicates that the B-integral is low enough not to have a strong effect on the pulse compression. Figure 10(d) shows the near-field image of the beam profile through the mirror leakage from the output of the compressor under full operation. The $1/e^2$ beam diameter is ~5.6 mm with an ellipticity of 0.93. The maximum peak power from the output of the picosecond laser system reaches up to more than 8 GW. By focusing the output beam with f/5.4 in air, we are able to easily observe a breakdown spark by bare eyes with an estimated threshold close to ~10^{14} W/cm^2 using the pulse energy of less than 1 mJ.

#236053 - $15.00 USD Received 11 Mar 2015; accepted 3 Apr 2015; published 10 Apr 2015

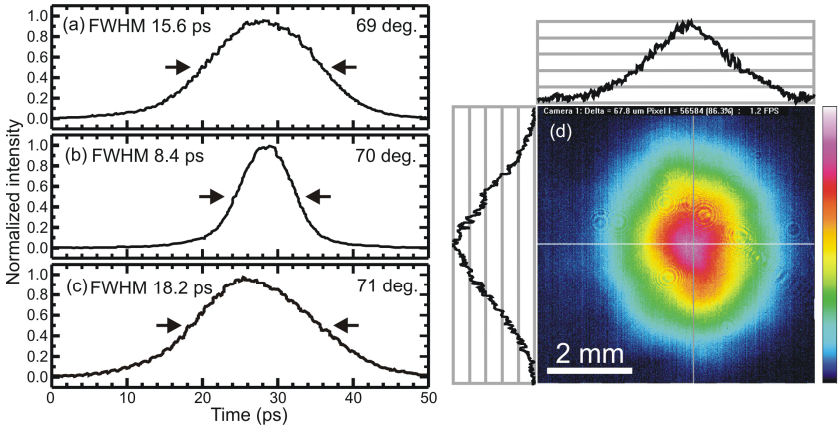

Fig. 10. The autocorrelation traces of the compressed pulse for the angle of incidence to the second grating which is (a) 69 degrees, (b) 70 degrees, and (c) 71 degrees. (d) The near-field image of the beam profile with the two-dimensional lineout from the output of compressor. FWHM durations are de-convolved pulse widths.

6. Conclusion

A high-energy, 1-kHz, ~1030-nm, picosecond, Yb-doped, hybrid CPA laser system with all optical synchronization to a Ti:sapphire seed oscillator is demonstrated with a compact pulse stretcher and compressor. The room-temperature front-end consists of multiple stages of SM YDFAs to pre-amplify a portion of the spectrum from an octave-spanning Ti:sapphire oscillator to nJ-level energy, and a room-temperature Yb:KYW RGA to increase the nJ seed to mJ-level while maintaining a broad spectral bandwidth for the two-stage cryogenic Yb:YAG MPA. The cryogenic Yb:YAG rod-type MPAs boost the 1.5-mJ energy from the RGA up to 70 mJ; the highest energy reported in a picosecond pulse among rod-type laser amplifiers at kHz repetition rates to the best of our knowledge. The pulse is compressed with 80% efficiency, and after compression has a nearly diffraction limited beam profile with M^2 = 1.2 and FWHM pulse duration of 5.9 ps, which represents a peak power of more than 8 GW. This hybrid amplifier approach provides a promising picosecond laser architecture to meet a host of requirements not only for industrial applications such as high-volume laser micro-machining, but also in scientific field, such as multi-color ultrabroadband OPCPA pumping via nonlinear frequency conversion and ultrafast X-ray generation via inverse Compton scattering.

Acknowledgments

We acknowledge technical support from Wenqian Ronny Huang and Hongyu Yang at MIT, and helpful discussions with Drs. Hüseyin Cankaya and Oliver D. Mücke at CFEL. This work was supported by AFOSR (FA9550-12-1-0499, FA9550-12-1-0080, FA9550-13-1-0159, and FA9550-14-1-0255), the Center for Free-Electron Laser Science, DESY, Germany, and the excellence cluster “The Hamburg Centre for Ultrafast Imaging—Structure, Dynamics and Control of Matter at the Atomic Scale” of the Deutsche Forschungsgemeinschaft. C.-L. Chang acknowledges the Ministry of Science and Technology in Taiwan for the Postdoctoral Research Abroad Program NSC 102-2917-I-564-026. P. Krogen acknowledges support by a NDSEG Graduate Fellowship. H. K. Liang acknowledges financial support from Singapore Institute of Manufacturing Technology (SIMT/14-110023) and Agency for Science, Technology and Research (A*STAR), Singapore.